Solute dispersion in channels with periodic square boundary roughness

Ivar Svalheim Haugerud, Gaute Linga, Eirik Grude Flekkøy

Angaben zur Veröffentlichung / Publication details:

Haugerud, Ivar Svalheim, Gaute Linga, and Eirik Grude Flekkøy. 2022. "Solute dispersion in channels with periodic square boundary roughness." *Journal of Fluid Mechanics* 944: A53. https://doi.org/10.1017/jfm.2022.522.

J. Fluid Mech. (2022), *vol*. 944, A53, doi:10.1017/jfm.2022.522

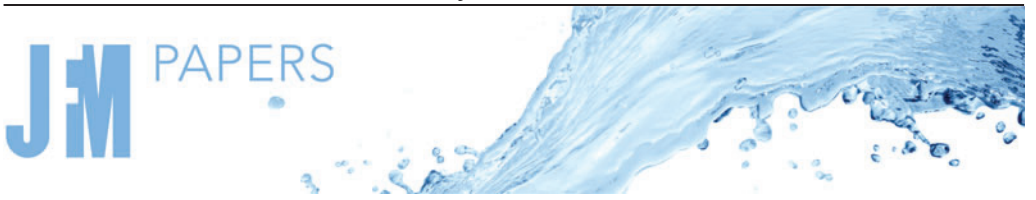

Solute dispersion in channels with periodic square boundary roughness

Ivar Svalheim Haugerud[1,2,†], **Gaute Linga**[1] **and Eirik Grude Flekkøy**[1]

[1]PoreLab, The Njord Centre, Department of Physics, University of Oslo, NO-0316 Oslo, Norway

[2]Mathematisch-Naturwissenschaftlich-Technische Fakultät, Institute of Physics, University of Augsburg, Universitätstr. 1, 86135 Augsburg, Germany

(Received 11 December 2021; revised 22 April 2022; accepted 2 June 2022)

Transport of solutes through channels with rough boundaries is abundant in natural and engineered settings. However, it is not known currently what the consequences of an abruptly alternating boundary are for the solute dispersion, in particular when advected by inertial fluid flow. To investigate this, we compute numerically the time-asymptotic longitudinal dispersion coefficient of a passive solute advected by fluid flow through a two-dimensional channel with square boundary roughness. We determine how the effective diffusion coefficient depends on the boundary amplitude, Péclet number and Reynolds number. For creeping flow, the effective diffusion coefficient is found to be enhanced significantly through the recirculation zones. Increasing fluid inertia reduces the effective diffusion coefficient by up to a factor of two for high Péclet numbers. We interpret this behaviour by analysing residence times computed from Lagrangian particle simulations.

Key words: dispersion

1. Introduction

Since the original work of Taylor (1953), the notion of an effective diffusion has proven to be extremely useful. His theory, and extensions thereof (Aris & Taylor 1956; Brenner 1980; Brenner & Adler 1982), has become the standard for estimating the dispersion in systems ranging from transport in blood (Goldstick, Ciuryla & Zuckerman 1976; Scow, Blanchette-Mackie & Smith 1976; Eckstein & Belgacem 1991) and groundwater systems (Desaulniers *et al.* 1986; Zheng & Wang 1999), sugar transport in plants (Jensen *et al.* 2009, 2016; Dölger *et al.* 2014), and the dispersion of airborne droplets for spreading in

† Email address for correspondence: ivar.haugerud@uni-a.de

disease transmission (Eames *et al.* 2009; Hui *et al.* 2009; Liu *et al.* 2017). Therefore, dispersion has been the focus of much experimental, numerical and theoretical research. The understanding of dispersion in axially invariant channels has since Taylor (1953) and Aris & Taylor (1956) been extended to allow for alternating fluid boundary conditions (Adrover & Cerbelli 2017; Adrover, Cerbelli & Giona 2018) and boundaries absorbing the solute (Levesque *et al.* 2012; Dagdug, Berezhkovskii & Skvortsov 2014). However, most channels and pores in natural and industrial systems are not perfectly flat. The addition of a varying boundary geometry is found to result in significant increase for the dispersion (Rosencrans 1997; Drazer *et al.* 2004; Schmidt, McCready & Ostafin 2005; Bolster, Dentz & Le Borgne 2009; Bouquain *et al.* 2012), and for certain systems even results in a decrease of the asymptotic spreading (Rosencrans 1997; Drazer *et al.* 2004; Bolster *et al.* 2009). Brenner's theory (Brenner 1980; Brenner & Adler 1982) has proven to be a solid theoretical framework for investigating such geometries (Bolster *et al.* 2009).

Most of the previous work with varying aperture has been done under certain idealized conditions, such as with potential flow (Eames & Bush 1999; Choi *et al.* 2005) or in the low-Reynolds-number regime where inertial effects can be ignored. Bolster *et al.* (2009) studied solute dispersion in channels with sinusoidal wall roughness under Stokes flow conditions. Here, the linearity of Stokes' equations and the analyticity of the boundary allowed for a perturbative approximation to the dispersion coefficient. Bouquain *et al.* (2012) built upon this work by investigating the effects of fluid inertia on the effective solute transport. Inertial effects can result in low-velocity regions called recirculation zones (RZ), which can trap the solute (Buonocore, Sen & Semperlotti 2020), resulting in a significant increase in the asymptotic spreading. While RZ can occur in Stokes flow, they become more dominant with increasing Reynolds number and appear for much smaller geometrical constraints.

Although the smooth single-wavelength roughness considered in a number of works (Laachi *et al.* 2007; Yariv & Dorfman 2007; Bolster *et al.* 2009; Bouquain *et al.* 2012) represents a major step towards real-world applications, the wall profiles found in both natural rock fractures (Cvetkovic, Selroos & Cheng 1999; Fiori & Becker 2015) and microfluidic devices such as the staggered herringbone mixer (Williams, Longmuir & Paul 2008; Ottino *et al.* 2004) do not obey the same smoothness, but contain jumps and often rugged shapes. Rough surfaces have been studied for purely diffusive transport (Mangeat, Guérin & Dean 2018), including geometries similar to those studied here (Kalinay & Percus 2010; Dagdug *et al.* 2021). With the addition of flow, recently Yoon & Kang (2021) applied advected random walk simulations to investigate the combined effect of a self-similar roughness and fluid inertia for a variety of advective transport rates. However, it was limited to the transient regime. Dagdug *et al.* (2014) studied how dispersion is affected by narrow dead ends where particles may be trapped for a finite time. Larger openings may lead to non-negligible flow inside the dead ends and non-trivial flow profiles. Further, the role of dead ends for diffusion with constant drift has been studied (Laachi *et al.* 2007; Berezhkovskii *et al.* 2010; Berezhkovskii & Dagdug 2011; Zitserman *et al.* 2014). However, this does not account for the role of fluid shear or Reynolds number. Despite the ubiquity of rough surfaces and high-inertia flows, it is unclear exactly how together they influence the effective diffusion. This is particularly important as numerous previous studies assume negligible flow in the stagnant areas or ignore fluid shear. The main novelty of this study is that we consider a geometry with sharply changing boundary roughness, resulting in large RZ. Previous studies of dispersion in channels of varying apertures have been limited to smooth boundaries (Bolster *et al.* 2009; Bouquain *et al.* 2012) or ignore both large openings and the flow inside the stagnant areas (Laachi *et al.* 2007; Berezhkovskii *et al.* 2010; Berezhkovskii & Dagdug 2011; Levesque *et al.* 2012;

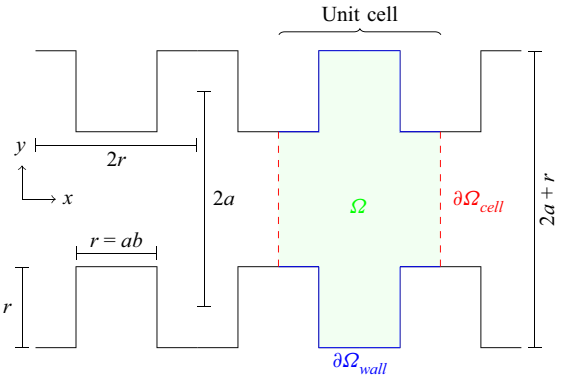

Figure 1. Illustration of the geometry considered in this paper. The quadratic square rough channel consists of infinitely many repeated unit cells, with channel height $2a + r$, unit cell width $2r$, and unit cell area $4a^2b$. The fluid unit cell boundary is created from the union of the unit cell boundary and wall boundary (2.8). The dimensionless square roughness $b \equiv r/a$ characterizes the geometry fully. For $b = 0$, one finds Aris' channel, and for $b = 2$, the channel is completely closed.

Dagdug *et al.* 2014; Zitserman *et al.* 2014). In this paper, we show that this boundary roughness leads to a qualitatively different behaviour compared to the aforementioned studies.

In order to understand this, we investigate systematically how a periodic discontinuous rough square boundary, illustrated in figure 1, influences the flow and effective diffusion of a passive solute in a two-dimensional channel. The channel is defined solely by the dimensionless boundary roughness amplitude b with average channel half-width a. The geometry is a simplified representation of generic rough-walled channels containing sharp notches and grooves of various sizes, e.g. discontinuous jumps in the boundary profile. The goal is to find and explain the effective diffusion coefficient's dependency on the boundary amplitude, Péclet and Reynolds number. The main result of the paper is a previously unobserved decrease in the effective diffusion coefficient with increasing Reynolds number, which is explained through the RZ trapping more solute particles into effectively stationary regions at larger Reynolds numbers, reducing the correlation time of horizontal solute transport.

The paper is organized as follows. In § 2, we summarize the necessary theory, and in § 3, we describe the geometry and numerical procedure underlying our computations. The results on flow fields and effective diffusion coefficients are presented in § 4, and in § 5 we summarize and conclude.

2. Theory

Passive transport of diffusive particles can be described by the evolution of the concentration field $C(\boldsymbol{r}, t)$ in space $\boldsymbol{r}$ and time t, which is governed by the advection–diffusion equation,

$$\partial_t C = Pe^{-1}\,\nabla^2 C - \boldsymbol{u}\cdot\nabla C. \tag{2.1}$$

The equation is written in dimensionless form, with incompressible flow and a constant molecular diffusion coefficient D_m. The Péclet number Pe is a dimensionless number that measures the advective versus diffusive transport rate $Pe \equiv aU/D_m$, where U is the average streamwise velocity and a is the mean channel half-width. The velocity field $\boldsymbol{u}$ is

determined by solving the steady incompressible Navier–Stokes equations

$$\boldsymbol{u}\cdot\boldsymbol{\nabla}\boldsymbol{u} = -\boldsymbol{\nabla}P + Re^{-1}\,\nabla^2\boldsymbol{u} + \boldsymbol{f}, \quad \boldsymbol{\nabla}\cdot\boldsymbol{u} = 0. \tag{2.2a,b}$$

Here, P is the pressure, and $\boldsymbol{f}$ is an external horizontal body force. The equation is written in dimensionless form, with the Reynolds number Re relating the inertial and viscous forces defined as $Re \equiv Ua/\nu$, where ν is the kinematic viscosity. To achieve a stationary velocity field, necessary for the application of Brenner's theory, the time-derivative term in the Navier–Stokes equations is ignored. For the simulations at $Re = 0$, we also neglect the nonlinear term $\boldsymbol{u}\cdot\boldsymbol{\nabla}\boldsymbol{u}$.

By solving (2.1) without flow and geometric constraints, one finds that the positional variance of the concentration σ^2 in a given direction grows linearly in time with slope $2D_m$. The effective diffusion coefficient parallel to the flow in d dimensions, with x being the streamwise spatial coordinate, can therefore be defined as

$$\sigma_\parallel^2(t) \equiv \int_{\mathbb{R}^d} x^2\,P(\boldsymbol{r})\,\mathrm{d}^d\boldsymbol{r} - \left(\int_{\mathbb{R}^d} x\,P(\boldsymbol{r})\,\mathrm{d}^d\boldsymbol{r}\right)^2 \equiv 2D_\parallel t, \tag{2.3}$$

where the probability P is the normalized concentration. The linear scaling is expected to hold when the solute has traversed the channel height multiple times, i.e. when $a^2/D_m \ll t$. The effective diffusion coefficient $D_\parallel$ will depend on the flow and geometry.

Brenner (1980) devised a general theoretical framework for calculating the effective diffusion coefficient in an arbitrary periodic geometry with steady incompressible flow. In this theory, the effective diffusion coefficient for dispersion along x can be found by calculating

$$D_\parallel = D_m\left\langle 1 - 2\,\frac{\partial\chi}{\partial x} + |\boldsymbol{\nabla}\chi|^2\right\rangle, \tag{2.4}$$

where the angle brackets denote a spatial average, defined in two dimensions as

$$\langle f\rangle = \frac{1}{V_\Omega}\int_\Omega f(\boldsymbol{r})\,\mathrm{d}\boldsymbol{r}^2, \tag{2.5}$$

with V_Ω being the volume of the unit cell. The scalar field χ is the solution of the equation

$$\nabla^2\chi - Pe\,\boldsymbol{u}\cdot\boldsymbol{\nabla}\chi = Pe\,\hat{\boldsymbol{x}}\cdot\boldsymbol{u}', \tag{2.6}$$

where $\hat{\boldsymbol{x}}$ is the unit vector in the streamwise direction, and $\boldsymbol{u}'$ is the velocity profile in the reference frame following the mean velocity, $\boldsymbol{u}' = \boldsymbol{u} - \langle\boldsymbol{u}\rangle$. The scalar field must also satisfy the boundary condition

$$\hat{\boldsymbol{n}}\cdot\boldsymbol{\nabla}\chi = -\hat{\boldsymbol{n}}\cdot\hat{\boldsymbol{x}} \quad \text{on } \partial\Omega_{wall}. \tag{2.7}$$

The solution must also be periodic on $\partial\Omega_{cell}$, which together with $\partial\Omega_{wall}$ constitutes the boundary of the unit cell:

$$\partial\Omega = \partial\Omega_{cell}\cup\partial\Omega_{wall}. \tag{2.8}$$

This is illustrated in figure 1. Additionally, we may remove the gauge freedom in χ by requiring $\langle\chi\rangle = 0$.

Brenner's result is a generalization of Aris' solution (Aris & Taylor 1956), which is valid only for axially invariant channels. Axially invariant geometry results in a horizontal velocity field $\boldsymbol{u} = u_x\hat{\boldsymbol{x}}$, and χ becoming independent of x, i.e. $\chi(\boldsymbol{r}) = \chi(\boldsymbol{r}_\perp)$, where

the subscript $\perp$ denotes the coordinates orthogonal to the flow direction. From these simplifications, we find a special case of Brenner's equation (2.4),

$$D_{\parallel}^{Aris} = D_m \left(1 + \left\langle |\nabla_{\perp}\chi(\boldsymbol{r}_{\perp})|^2 \right\rangle\right), \tag{2.9}$$

where the scalar field is the solution of the simpler equation

$$\nabla_{\perp}^2 \chi = Pe\, \hat{\boldsymbol{x}} \cdot \boldsymbol{u}'. \tag{2.10}$$

By introducing the dimensionless quantity ϕ through $\chi = a\, Pe\, \phi$, (2.9) becomes

$$D_{\parallel}^{Aris} = D_m \left[1 + Pe^2 \left\langle |\nabla\phi|^2 \right\rangle\right]. \tag{2.11}$$

By defining a geometric factor $\kappa = \left\langle |\nabla\phi|^2 \right\rangle$, the result can be written identically to Aris' expression (Aris & Taylor 1956, p. 75), with $\kappa = 2/105$ for a straight two-dimensional channel.

To simulate the trajectories of the diffusive passive tracers and verify independently the theoretical predictions made with Brenner's theory, advected random walk simulations are used (Bolster *et al.* 2009, 2014; Giona, Venditti & Adrover 2020). The discretization method, boundary conditions and numerical implementation are discussed in Appendix A.

3. Velocity fields, geometry and problem setup

Following the result from Aris (Aris & Taylor 1956), among others (Bolster *et al.* 2009; Bouquain *et al.* 2012), we represent the effective diffusion coefficient in the form

$$D_{\parallel} = D_m \left(\frac{d_m^{\parallel}(b)}{D_m} + \kappa\, Pe^2\, g\,(Pe, Re, b)\right). \tag{3.1}$$

The geometric factor g measures the effect of fluid flow on the asymptotic spreading as a function of the Péclet number, Reynolds number and roughness amplitude b. The constant κ is the geometric factor from the Taylor–Aris result, which for a two-dimensional straight channel takes the value $2/105$, such that $g(Pe, Re, 0) = 1$. We have further defined $d_m^{\parallel}(b)$ as the effective diffusion coefficient for pure diffusion at roughness b, such that one retrieves the correct value in the limit of zero Pe. The effective diffusion has therefore been decomposed into one term, $d_m^{\parallel}(b)$, representing the effect of horizontal purely diffusive transport that is important at small Péclet numbers, and another term representing the effect of flow, where a scaling of order Pe^2, similar to Taylor–Aris, is expected.

To understand dispersion phenomena in rough channels, the velocity field is found by solving numerically the incompressible time-independent Navier–Stokes equations for various boundary amplitudes and Reynolds numbers. After solving for the velocity profile, the Reynolds number is calculated and the flow is normalized to have horizontal unit cell average velocity 1. The Reynolds number is therefore changed by varying the kinematic viscosity ν. Different transport rates are investigated in a wide range of Péclet numbers, where the diffusion coefficient is varied upon the same velocity profile. By altering the diffusivity of momentum and mass, the Reynolds and Péclet numbers are changed independently. Hence the investigation is performed for various Schmidt numbers, defined as $Sc \equiv Pe/Re$. Experimentally, the Péclet number can remain fixed while increasing the

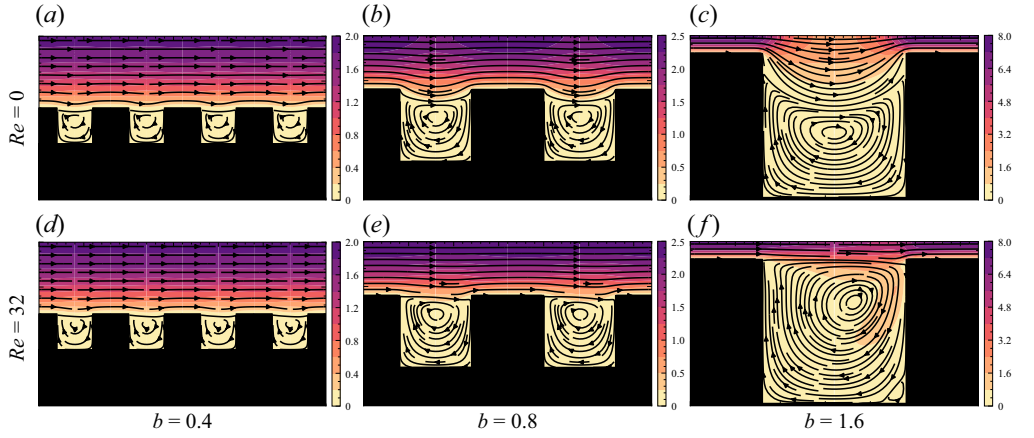

Figure 2. Visualization of the velocity fields at different roughnesses b and Reynolds numbers. For each panel, the spatial axes are scaled equally, and the colour bar denotes the fluid speed in factors of the unit cell average value. (a–c) Reynolds number 0, and roughness $b = 0.4$, 0.8 and 1.6, respectively. (d–f) Reynolds number 32, and roughness $b = 0.4$, 0.8 and 1.6, respectively.

Reynolds number by reducing the viscosity of the fluid, and increasing the average velocity to compensate for a larger molecular diffusivity. This can be seen from the Stokes–Einstein relation (Einstein 1905) where $D_m \propto 1/\nu$.

The study is purely numerical, primarily using the finite element method. Convergence is verified by ensuring that the average velocity and effective diffusion coefficient change by less than 1 % when doubling the spatial resolution of the finite element mesh. The code for the Navier–Stokes equations, Brenner's equation and diffusive passive tracers simulations are public through a designated GitHub repository (Haugerud 2022). The variational form of the equations is discussed in Appendix B.

4. Results

4.1. *Velocity field*

In figure 2, the streamlines in the bottom half of the unit cell are visualized for roughnesses $b = 0.4$, 0.8 and 1.6, for Reynolds numbers 0 (figure 2a–c) and $10^{1.5} \approx 32$ (figure 2d–f). For $b = 0.4$, the RZ are close to filling the full cavity area, independent of Reynolds number. With increasing roughness, the high-speed central streamlines move further into the cavities at low Re, reducing the relative size of the RZ. This does not occur for $Re = 32$, where the RZ fill the entire cavity area for all boundary amplitudes.

4.2. *Verification: comparisons between Brenner's solution and diffusive passive tracers*

The numerical implementation of the solver for Brenner's equations (2.6) and (2.7) is verified by comparing its predicted effective diffusion coefficient with those found using advected random walk simulations, as shown in figure 3. The comparison without flow, shown in figure 3(a), shows that the effective diffusion coefficient decreases linearly until around $b = 1$ with slope -0.42, and approaches zero when the channel is completely closed at $b = 2$. The result is compared further to the theories due to Fick–Jacobs (Jacobs 1935) and Dagdug *et al.* (2021). While Fick–Jacobs overestimates and Dagdug *et al.* underestimates the effective diffusion coefficient, the latter is much closer to the correct

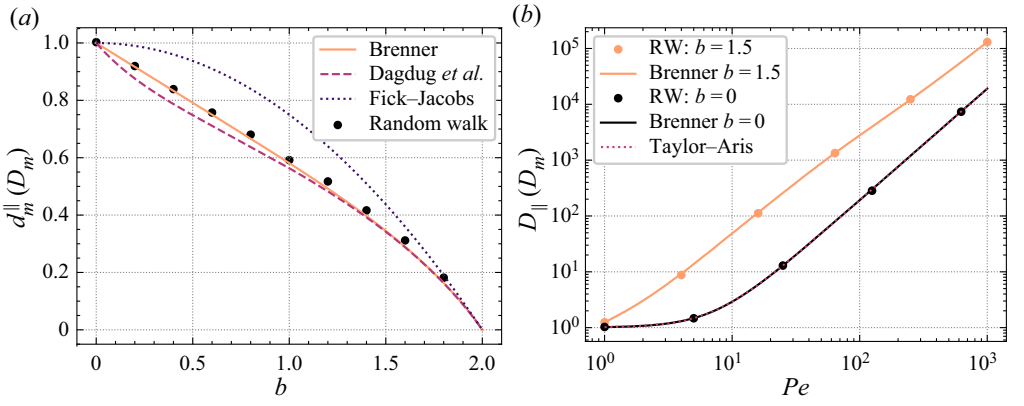

Figure 3. The effective diffusion coefficient (*a*) without advection and (*b*) with advection, at zero Reynolds number, found by different methods, i.e. solving Brenner's equation, random walk (RW) simulations and the analytic expressions from Fick–Jacobs (Jacobs 1935) and Dagdug *et al.* (2021).

values produced by Brenner's theory. This is understood by the former being valid only for slowly varying boundaries, and the latter being valid even for abruptly varying channel diameters (Dorfman & Yariv 2014). All methods agree when the narrowest channel width approaches zero, as the horizontal transport is then dominated by this portion of the channel. For the case with flow, shown in figure 3(*b*), the roughness results in a large increase for small values of the Péclet number, which approaches a scaling with the Péclet number similar to the Taylor–Aris expression (2.11). For $b = 0$, the results also agree with the Taylor–Aris result. Based on this, we have established that the Brenner equations solver produces the correct effective diffusion coefficient. For the following results, the Brenner equations solver is used, as it is exact and computationally much more efficient than advected random walk simulations.

4.3. *Effective diffusion for creeping flow*

With a verified solver of Brenner's equations, the effective diffusion coefficient is calculated as a function of both the Péclet number and the roughness at creeping flow. The form of the geometric factor g, defined in (3.1), at Stokes flow conditions ($Re = 0$) is displayed as functions of Péclet number and roughness in figure 4. The figure shows that increasing the roughness always results in more efficient spreading, but the effect is diminished at higher Péclet numbers. Furthermore, the geometric factor is always larger than 1, meaning that an increase in the amplitude b always increases the dispersion due to flow. For very large Péclet numbers, g moves closer to 1, i.e. more similar to the Taylor–Aris result.

Even though the geometric factor is always larger than 1, the effective diffusion is not necessarily larger than the Taylor–Aris result from (2.11). In figure 5, the relative change in the dispersion from Poiseuille flow to our geometry, defined as

$$\Delta D_{\parallel} \equiv \frac{D_{\parallel}(Pe, b, Re = 0) - D_{\parallel}^{aris}(Pe)}{D_{\parallel}^{aris}(Pe)}, \tag{4.1}$$

is displayed. A slight decrease is observed when both transport mechanisms are of equal importance, $Pe = 1$, due to the horizontal diffusive spreading being limited by the varying

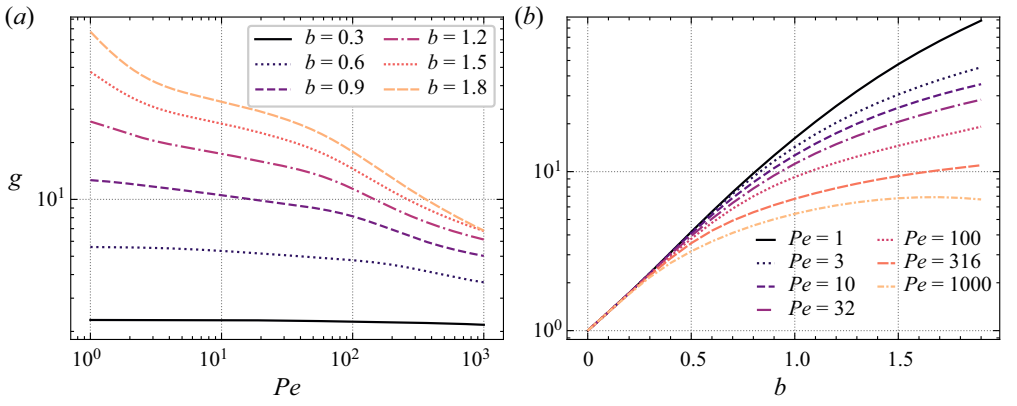

Figure 4. At Reynolds number 0, the geometric factor (3.1) as functions of (*a*) Péclet number and (*b*) boundary roughness.

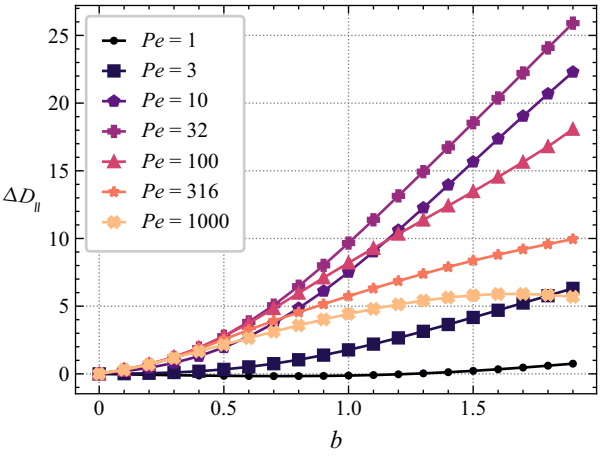

Figure 5. At Reynolds number 0, the relative change in the effective diffusion coefficient (4.1), compared to the Taylor–Aris result, is positive except at $Pe = 1$.

boundary amplitude. This is true only for small boundary amplitudes, and the relative change becomes positive at around $b = 1.25$. The relative change is maximized for an intermediate value $Pe = 32$. Except for $Pe = 10^3$, the relative change is largest for the largest boundary amplitude.

4.4. *Effective diffusion with fluid inertia*

The effect of fluid inertia on $D_\parallel$ is displayed in figure 6, through its relative change from creeping flow to a non-zero Reynolds number:

$$\Delta D_\parallel^{Re} \equiv \frac{D_\parallel(Pe, b, Re) - D_\parallel(Pe, b, Re = 0)}{D_\parallel(Pe, b, Re = 0)}. \tag{4.2}$$

For each panel of figure 6, the Péclet number is constant, while changing the flow through the roughness and Reynolds number. For small roughnesses the relative change is zero, independent of the Reynolds and Péclet numbers. When the two transport mechanisms

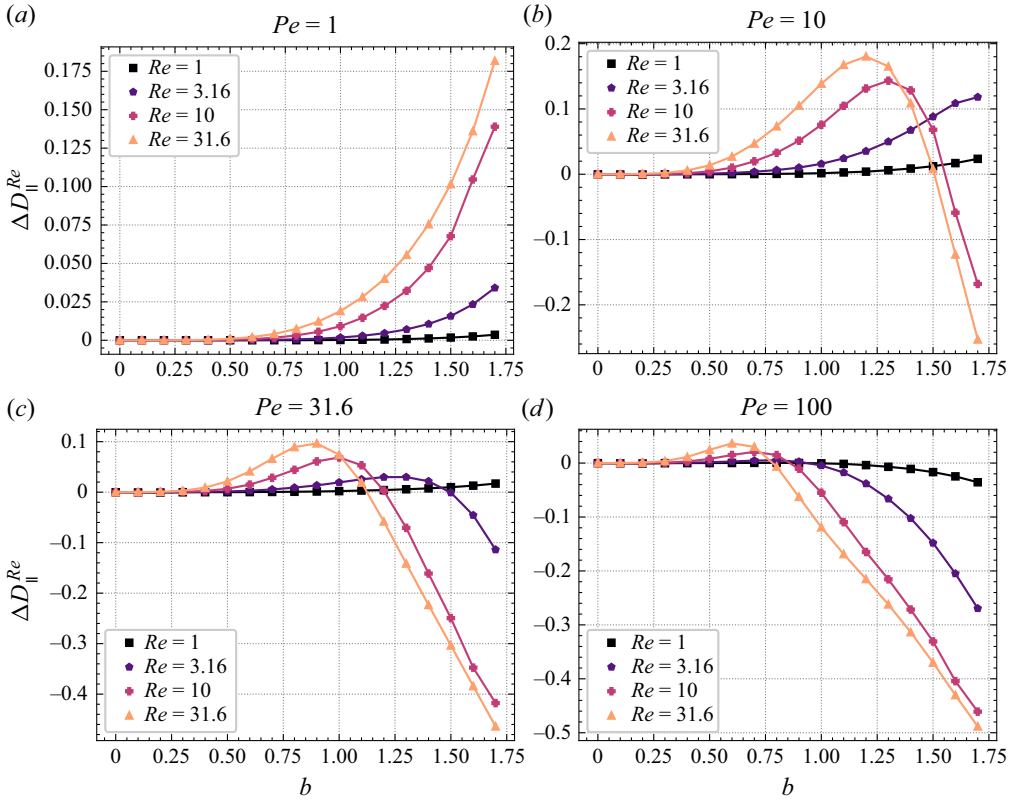

Figure 6. The relative change in the effective diffusion coefficient with Reynolds number (4.2) is displayed for a constant Péclet number, while changing the flow through the roughness and Reynolds number.

are of equal importance, an increase in the Reynolds number increases the spreading, and this is further magnified with increasing roughness. On the contrary, for high Péclet numbers, the same change in flow decreases the value of the effective diffusion coefficient by as much as 50 %. The consequence of fluid inertia is therefore highly dependent on the relative transport rates.

4.5. *Residence times of diffusive passive tracers*

By analysing the positions and trajectories of the diffusive passive tracers, a physical explanation for the behaviour observed above can be found. We are especially interested in understanding how an increase in Reynolds number can increase or decrease the effective diffusion, depending on the Péclet number. Therefore, the simulations are performed at creeping flow and $Re = 32$ – the same values for which the streamlines in figure 2 are displayed. Three different orders of magnitudes of the Péclet number are also investigated, 1, 10 and 100, corresponding to three of the graphs in figure 6.

By finding the shape of the RZ, the average number of particles in the RZ is measured and displayed in figure 7. The proportion of particles always increases for creeping flow, although the slope decreases for the largest boundaries. For Reynolds number 32, on the other hand, the linear increase matches the fact that the RZ fill the whole cavity area. This behaviour is consistent with the behaviour of the RZ area, inferred from figure 2. For both

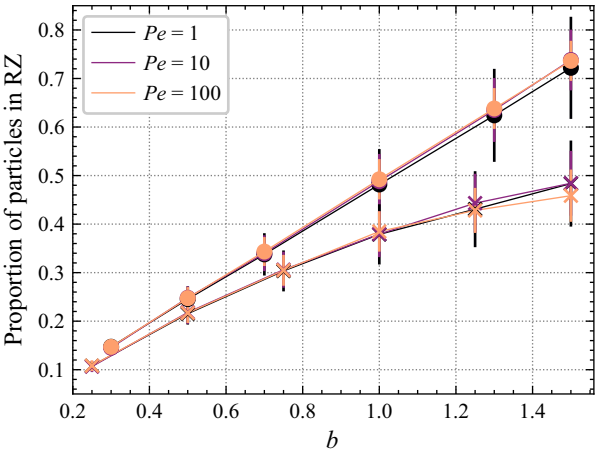

Figure 7. The average number of particles in RZ for $Re = 0$ (crosses) and $Re = 32$ (dots) is displayed versus boundary roughness for a variety of Péclet numbers.

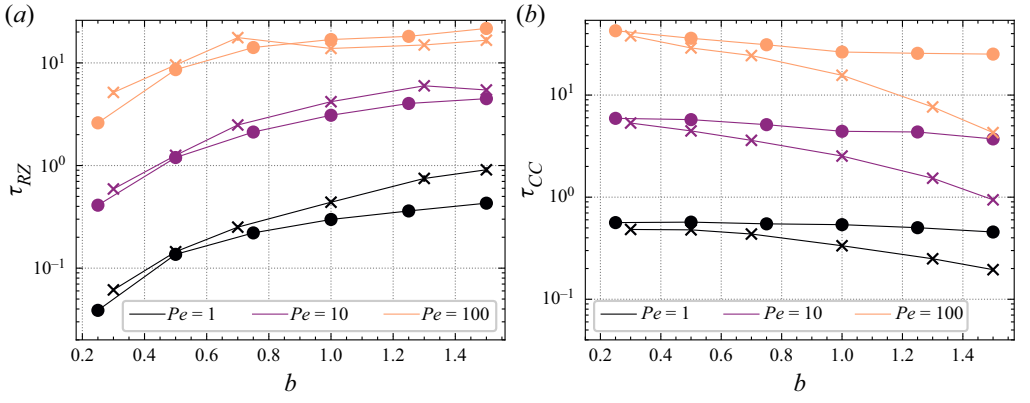

Figure 8. The characteristic residence times in (a) the recirculation zones τ_{RZ}, and (b) the central channel τ_{CC}, for both creeping flow (dots) and inertial flow with $Re = 32$ (crosses), with boundary roughness for a variety of Péclet numbers.

cases, the effect of changing the Péclet number is negligible compared to the fluctuations around the averaged values, as one would expect.

The probability density of residence times in the RZ and the central channel (CC) decays exponentially as $P(t) = \exp(-t/\tau_i)$ for $i \in \{CC, RZ\}$. For the set of Péclet numbers, Reynolds numbers and roughnesses investigated above, the behaviour of the characteristic residence times τ_{CC}, τ_{RZ} are displayed in figure 8. With increasing Péclet number, the residence times in both the CC and the RZ increase due to the diffusive transport between the two regions diminishing. With a larger roughness, the RZ area increases and the CC area decreases, resulting in the same behaviour with their corresponding residence times. Increasing fluid inertia has a minimal effect on the RZ residence time, but drastically decreases the CC residence time, especially at large boundary amplitudes.

5. Discussion

To achieve a large value of the effective diffusion, the average autocorrelation time for the advected horizontal velocity should be maximized, with a broad distribution in advection speed between particles (Bolster *et al.* 2009). This can also be realized from the Taylor–Green–Kubo relation (Taylor 1922; Green 1951; Kubo 1957), which is an alternative way of retrieving the dispersion coefficient $D_{\parallel} = \int_0^\infty C_v(t)\,\mathrm{d}t$, where $C_v = \overline{u_x'(t), u_x'(0)}$ is the ensemble averaged autocorrelation function for the streamwise Lagrangian velocity of the particles. A varying boundary geometry can result in a decrease in the effective diffusion coefficient due to the autocorrelation time being reduced with enhanced vertical diffusive transport at the pore throats. It can equally well increase due to the width of the velocity distribution increasing with additional fluid shear and RZ. This has been studied for smoothly varying boundary amplitudes (Bolster *et al.* 2009; Bouquain *et al.* 2012), where a threshold value of the boundary amplitude is necessary for RZ to appear. RZ are present at all boundary amplitudes for the discontinuous geometry studied here, resulting in an effective diffusion coefficient larger than the Taylor–Aris result even at small boundary amplitudes, as shown in figure 5.

We observe that the geometric factor comes closer to the Taylor–Aris result for higher Péclet numbers, as seen in figure 4. The effect occurs at all roughnesses, but is enhanced at larger values. This result can seem surprising, as the Péclet number increases the importance of the flow field, which is highly dependent on the geometry. The behaviour can be understood from the characteristic residence time in both the CC and RZ scaling as Pe^{α} with $\alpha < 1$ as seen in figure 8. This means that transitions between the CC and RZ are larger than what would be expected from the same change in the molecular diffusivity without flow, effectively reducing the correlation time, hence the geometric factor decreases.

Figure 2 shows that at large Re, the open streamlines of the CC occupy a smaller area over the RZ than they do at small Re. For this reason, the typical distance that a particle needs to diffuse in order to pass from open to closed streamlines is reduced with increasing Re. This explains the decrease in the CC occupation times with Reynolds number, as seen in figure 8. The increased accessibility of the RZ, decreasing the correlation time in the CC, governs the change of $D_{\parallel}$ with Re and b.

Two competing effects give rise to the changes with Reynolds number observed in figure 6. On the one hand, when particles get stuck in the RZ, their distance to the particles moving in the CC increases quickly. This enhances the dispersion. On the other hand, the particles that get stuck in the RZ deplete the population of particles that move on the open streamlines. When the CC is depleted by a reduced mean residence time in the CC, the dispersion is reduced as the correlation time decreases.

The observed decrease in $D_{\parallel}$ with Reynolds number disagrees with both Bouquain *et al.* (2012) and Bolster *et al.* (2009), who postulate a monotonic relationship between $D_{\parallel}$ and Re. While this relationship has been observed for the smooth geometries in their investigation, it does not appear to extend to discontinuous geometries.

For the linear regime in figure 7, the velocity profile is similar to that of Poiseuille flow in the CC, with lid-driven flow in the cavity. The dynamics may therefore be captured by modelling the RZ as stationary areas, where the exact shape of the RZ is not of importance, only their accessibility and characteristic residence time. Analytical expressions might be achievable through effective models, specifically along the lines of Levesque *et al.* (2012) and Dagdug *et al.* (2014). The model by Dagdug *et al.* (2014) may be a good starting point; however, in its current form it is insufficient to model our system, because the square

boundary roughness violates their assumptions of narrow cavity (dead-end) openings not affecting the main channel flow and the assumption of no flow inside the cavities. Our simulations indicate that it remains a challenge to model the complex dependence of the residence times on Re, Pe and b.

A recent publication by Yoon & Kang (2021) focused on dispersion under the combined effect of self-similar rough surfaces and fluid inertia. Their investigation found that the increase of roughness and Reynolds number can increase or decrease the transport, depending on the Péclet number. When advective transport was dominating, $Pe = 10^5$, their channel is flushed efficiently due to RZ not being entered by the random walk. The RZ are not entered at advected-dominated transport due to the region separating the RZ and the CC acting as a slip boundary moving at a large velocity. In the asymptotic regime, RZ will necessarily be entered, and their findings are therefore valid only in the transient regime. The dynamics behind the transport efficiency increasing or decreasing depending on the Péclet number found here is therefore different from that found by Yoon & Kang (2021).

6. Conclusion

In this paper we have investigated numerically the spreading of solutes in rough channels, considering a periodic square boundary roughness as a prototype for the discontinuous roughness profiles found in fractures and microfluidic devices. The purpose of the work was to understand how the combination of a discontinuous boundary and fluid inertia could influence solute dispersion.

By comprehensive numerical simulations using Brenner's theoretical framework (Brenner 1980), we have mapped out the dependence of the effective diffusion coefficient on Péclet number, Reynolds number and the amplitude of the discontinuous roughness. The most important findings, compared to the established knowledge on flow in channels with smoothly varying apertures, can be summarized in the following two points.

(i) The effect of a discontinuous boundary is seen in the velocity field for Stokes flow, as RZ are present for small boundary amplitudes, unlike what is observed for smooth boundaries (Bolster *et al.* 2009). This, in turn, results in an increase in the effective diffusion for all boundary amplitudes, making the effective diffusivity more than an order of magnitude larger than the Taylor–Aris result.

(ii) The relative change of the effective diffusion coefficient with the Reynolds number is found to be able to either increase or decrease depending on the Péclet number. For large boundary amplitudes, the relative change is positive for small Péclet numbers, and negative for large Péclet numbers. This effect is contrary to what is observed for smooth boundaries (Bolster *et al.* 2009; Bouquain *et al.* 2012). In this paper, through measurements of residence times in the RZ and in the main channel, we have made the case that this is due to the accessibility and size of the RZ increasing with the Reynolds number, reducing the correlation time in the CC significantly at small diffusive transport rates. This represents our main result.

Acknowledgements. We thank K.S. Olsen for fruitful discussions on diffusion in complex geometries.

Funding. This work was supported by the Research Council of Norway through its Centers of Excellence funding scheme (project no. 262644, PoreLab CoE) and FRINATEK scheme (G.L., E.G.F., project no. 325819, 'Mixing in multiphase flows through microporous media').

Declaration of interests. The authors report no conflict of interest.

Author ORCIDs.
Ivar Svalheim Haugerud https://orcid.org/0000-0001-9931-3741;
Gaute Linga https://orcid.org/0000-0002-0987-8704;
Eirik Grude Flekkøy https://orcid.org/0000-0002-6141-507X.

Appendix A. Advected random walkers

Advected random walkers follow the Langevin equation on a background velocity field

$$\frac{\mathrm{d}\boldsymbol{r}_k}{\mathrm{d}t} = \boldsymbol{u}(\boldsymbol{r}_k(t)) + \boldsymbol{\xi}_k(t), \tag{A1}$$

where k denotes the particle index. Each component i of the noise vector ξ_k follows a directionally unbiased and uncorrelated Gaussian distribution with width proportional to the diffusion coefficient:

$$\langle \xi_{i,k} \rangle = 0, \quad \langle \xi_{i,k}(t)\, \xi_{j,l}(t') \rangle = 2D_m \delta_{ij} \delta_{kl} \delta(t - t'), \tag{A2}$$

where i denotes the spatial direction, and both the Kronecker-delta and Dirac-delta are used. Using the Itô formalism (Mannella & McClintock 2012), this is integrated to find the numerical updating scheme

$$\boldsymbol{r}_k(t + \Delta t) = \boldsymbol{r}_k(t) + \boldsymbol{u}(\boldsymbol{r}_k(t))\, \Delta t + \boldsymbol{\eta}_k \sqrt{2D_m\, \Delta t}, \tag{A3}$$

where Δt is the numerical time step of the random walkers, and $\boldsymbol{\eta}$ is a vector of uncorrelated random numbers drawn from a Gaussian distribution with mean 0 and variance 1. Numerically, we first compute the velocity field by a finite element method and then perform the updating scheme for the random walkers by using the interpolated velocity field. A bounce-back boundary condition is used for the particles, where they move back to their previous position if they move out of the fluid domain. The code can be found in a designated GitHub repository (Haugerud 2022).

Appendix B. Variational form and finite element scheme

To use the finite element method, the variational formulation of the equation must be found. This is done by multiplying the equation by an arbitrary test function v and performing a volume integral over the domain Ω. Through integration by parts, double or higher-order derivatives must be removed. Following this procedure yields the variational form of the dimensionless Navier–Stokes equations (2.2*a*,*b*):

$$Re \int_\Omega v u_j \nabla_j u_i + \int_\Omega \nabla_j u_i \nabla_j v - \int_\Omega P \nabla_i v = \int_\Omega f_i v + \int_{\partial \Omega_{wall}} v \hat{n}_j \nabla_j u_i, \tag{B1}$$

where the no-slip Dirichlet boundary condition for the velocity field is applied at the boundary wall. Additionally, the incompressibility of the fluid (2.2*a*,*b*) should be solved

simultaneously:

$$\int_{\Omega} q \nabla_i u_i = 0, \tag{B2}$$

where the test function for this equation is denoted by q. The Neumann boundary conditions for Brenner's equation (2.7) are included through the variational form

$$Pe \int_{\Omega} v u_i \nabla_i B + \int_{\Omega} \nabla_i B \nabla_i v = -Pe \int_{\Omega} u_x' v + \int_{\partial \Omega_{wall}} \hat{n}_i \hat{x}_i v. \tag{B3}$$

In our numerical implementation, kth degree piecewise polynomials (Lagrange elements) P_k are used as basis functions. When solving the Navier–Stokes equations, P_3 elements have been used for the velocity field, and P_2 elements have been used for the pressure in order to satisfy the Babuška–Brezzi condition (Langtangen, Mardal & Winther 2002), and P_2 elements are also used to solve for the Brenner field. To solve the equations, the FEniCS package (Logg, Mardal & Wells 2012) is used, which efficiently assembles and solves both nonlinear and linear variational problems. For a more detailed description, we refer to the GitHub repository (Haugerud 2022).

References

Adrover, A. & Cerbelli, S. 2017 Laminar dispersion at low and high Peclet numbers in finite-length patterned microtubes. *Phys. Fluids* **29** (6), 062005.

Adrover, A., Cerbelli, S. & Giona, M. 2018 Taming axial dispersion in hydrodynamic chromatography columns through wall patterning. *Phys. Fluids* **30** (4), 042002.

Aris, R. & Taylor, G.I. 1956 On the dispersion of a solute in a fluid flowing through a tube. *Proc. R. Soc. Lond.* A **235** (1200), 67–77.

Berezhkovskii, A.M. & Dagdug, L. 2011 Analytical treatment of biased diffusion in tubes with periodic dead ends. *J. Chem. Phys.* **134** (12), 124109.

Berezhkovskii, A.M., Dagdug, L., Makhnovskii, Y.A. & Zitserman, V.Y. 2010 Communications: drift and diffusion in a tube of periodically varying diameter. Driving force induced intermittency. *J. Chem. Phys.* **132** (22), 221104.

Bolster, D., Dentz, M. & Le Borgne, T. 2009 Solute dispersion in channels with periodically varying apertures. *Phys. Fluids* **21** (5), 056601.

Bolster, D., Méheust, Y., Le Borgne, T., Bouquain, J. & Davy, P. 2014 Modeling preasymptotic transport in flows with significant inertial and trapping effects – the importance of velocity correlations and a spatial Markov model. *Adv. Water Resour.* **70**, 89–103.

Bouquain, J., Méheust, Y., Bolster, D. & Davy, P. 2012 The impact of inertial effects on solute dispersion in a channel with periodically varying aperture. *Phys. Fluids* **24** (8), 083602.

Brenner, H. 1980 Dispersion resulting from flow through spatially periodic porous media. *Phil. Trans. R. Soc. Lond.* A **297** (1430), 81–133.

Brenner, H. & Adler, P.M. 1982 Dispersion resulting from flow through spatically periodic porous media II. Surface and intraparticle transport. *Phil. Trans. R. Soc. Lond.* A **307** (1498), 149–200.

Buonocore, S., Sen, M. & Semperlotti, F. 2020 Stochastic scattering model of anomalous diffusion in arrays of steady vortices. *Proc. R. Soc.* A **476** (2238), 20200183.

Choi, J., Margetis, D., Squires, T.M. & Bazant, M.Z. 2005 Steady advection–diffusion around finite absorbers in two-dimensional potential flows. *J. Fluid Mech.* **536**, 155–184.

Cvetkovic, V., Selroos, J.O. & Cheng, H. 1999 Transport of reactive tracers in rock fractures. *J. Fluid Mech.* **378**, 335–356.

Dagdug, L., Berezhkovskii, A.M. & Skvortsov, A.T. 2014 Aris–Taylor dispersion in tubes with dead ends. *J. Chem. Phys.* **141** (2), 024705.

Dagdug, L., Berezhkovskii, A.M., Zitserman, V.Y. & Bezrukov, S.M. 2021 Effective diffusivity of a Brownian particle in a two-dimensional periodic channel of abruptly alternating width. *Phys. Rev.* E **103** (6), 062106.

Desaulniers, D.E., Kaufmann, R.S., Cherry, J.A. & Bentley, H.W. 1986 37Cl-35Cl variations in a diffusion-controlled groundwater system. *Geochim. Cosmochim. Acta* **50** (8), 1757–1764.

DÖLGER, J., RADEMAKER, H., LIESCHE, J., SCHULZ, A. & BOHR, T. 2014 Diffusion and bulk flow in phloem loading: a theoretical analysis of the polymer trap mechanism for sugar transport in plants. *Phys. Rev.* E **90** (4), 042704.

DORFMAN, K.D. & YARIV, E. 2014 Assessing corrections to the Fick–Jacobs equation. *J. Chem. Phys.* **141** (4), 044118.

DRAZER, G., AURADOU, H., KOPLIK, J. & HULIN, J.P. 2004 Self-affine fronts in self-affine fractures: large and small-scale structure. *Phys. Rev. Lett.* **92** (1), 014501.

EAMES, I. & BUSH, J.W.M. 1999 Longitudinal dispersion by bodies fixed in a potential flow. *Proc. R. Soc. Lond.* A **455** (1990), 3665–3686.

EAMES, I., TANG, J.W., LI, Y. & WILSON, P. 2009 Airborne transmission of disease in hospitals. *J. R. Soc. Interface* **6** (suppl_6), S697–S702.

ECKSTEIN, E.C. & BELGACEM, F. 1991 Model of platelet transport in flowing blood with drift and diffusion terms. *Biophys. J.* **60** (1), 53–69.

EINSTEIN, A. 1905 Über die von der molekularkinetischen Theorie der Wärme geforderte Bewegung von in ruhenden Flüssigkeiten suspendierten Teilchen. *Ann. Phys.* **322** (8), 549–560.

FIORI, A. & BECKER, M.W. 2015 Power law breakthrough curve tailing in a fracture: the role of advection. *J. Hydrol.* **525**, 706–710.

GIONA, M., VENDITTI, C. & ADROVER, A. 2020 On the long-term simulation of stochastic differential equations for predicting effective dispersion coefficients. *Physica* A **543**, 123392.

GOLDSTICK, T.K., CIURYLA, V.T. & ZUCKERMAN, L. 1976 Diffusion of oxygen in plasma and blood. In *Oxygen Transport to Tissue – II* (ed. J. Grote, D. Reneau & G. Thews), Advances in Experimental Medicine and Biology, vol. 75, pp. 183–190. Springer.

GREEN, M.S. 1951 Brownian motion in a gas of noninteracting molecules. *J. Chem. Phys.* **19** (8), 1036–1046.

HAUGERUD, I. 2022 Brenner dispersion in rough channels. https://github.com/ivarhaugerud/Brenner_dispersion_rough_channels, accessed: 2022-04-05.

HUI, D.S., CHOW, B.K., CHU, L.C.Y., NG, S.S., HALL, S.D., GIN, T. & CHAN, M.T.V. 2009 Exhaled air and aerosolized droplet dispersion during application of a jet nebulizer. *Chest* **135** (3), 648–654.

JACOBS, M.H. 1935 Diffusion processes. In *Diffusion Processes* (ed. M.H. Jacobs), pp. 1–145. Springer.

JENSEN, K.H., BERG-SØRENSEN, K., BRUUS, H., HOLBROOK, N.M., LIESCHE, J., SCHULZ, A., ZWIENIECKI, M.A. & BOHR, T. 2016 Sap flow and sugar transport in plants. *Rev. Mod. Phys.* **88** (3), 035007.

JENSEN, K.H., RIO, E., HANSEN, R., CLANET, C. & BOHR, T. 2009 Osmotically driven pipe flows and their relation to sugar transport in plants. *J. Fluid Mech.* **636**, 371–396.

KALINAY, P. & PERCUS, J.K. 2010 Mapping of diffusion in a channel with abrupt change of diameter. *Phys. Rev.* E **82** (3), 031143.

KUBO, R. 1957 Statistical-mechanical theory of irreversible processes. I. General theory and simple applications to magnetic and conduction problems. *J. Phys. Soc. Japan* **12** (6), 570–586.

LAACHI, N., KENWARD, M., YARIV, E. & DORFMAN, K.D. 2007 Force-driven transport through periodic entropy barriers. *Europhys. Lett.* **80** (5), 50009.

LANGTANGEN, H.P., MARDAL, K.-A. & WINTHER, R. 2002 Numerical methods for incompressible viscous flow. *Adv. Water Resour.* **25**, 1125–1146.

LEVESQUE, M., BÉNICHOU, O., VOITURIEZ, R. & ROTENBERG, B. 2012 Taylor dispersion with adsorption and desorption. *Phys. Rev.* E **86** (3), 036316.

LIU, L., WEI, J., LI, Y. & OOI, A. 2017 Evaporation and dispersion of respiratory droplets from coughing. *Indoor Air* **27** (1), 179–190.

LOGG, A., MARDAL, K.-A. & WELLS, G. (Eds) 2012 *Automated Solution of Differential Equations by the Finite Element Method*. Lecture Notes in Computational Science and Engineering, vol. 84. Springer, 1–741.

MANGEAT, M., GUÉRIN, T. & DEAN, D.S. 2018 Dispersion in two-dimensional periodic channels with discontinuous profiles. *J. Chem. Phys.* **149** (12), 124105.

MANNELLA, R. & MCCLINTOCK, P. 2012 Itô versus Stratonovich: 30 years later. *Fluct. Noise Lett.* **11**, 1–10.

OTTINO, J.M., WIGGINS, S.R., STROOCK, A.D. & MCGRAW, G.J. 2004 Investigation of the staggered herringbone mixer with a simple analytical model. *Phil. Trans. R. Soc. Lond.* A **362** (1818), 971–986.

ROSENCRANS, S. 1997 Taylor dispersion in curved channels. *SIAM J. Appl. Maths* **57**, 1216–1241.

SCHMIDT, S.M., MCCREADY, M.J. & OSTAFIN, A.E. 2005 Effect of oscillating fluid shear on solute transport in cortical bone. *J. Biomech.* **38** (12), 2337–2343.

SCOW, R.O., BLANCHETTE-MACKIE, E.J. & SMITH, L.C. 1976 Role of capillary endothelium in the clearance of chylomicrons. A model for lipid transport from blood by lateral diffusion in cell membranes. *Circul. Res.* **39** (2), 149–162.

TAYLOR, G.I. 1922 Diffusion by continuous movements. *Proc. Lond. Math. Soc.* **s2-20** (1), 196–212.

TAYLOR, G.I. 1953 Dispersion of soluble matter in solvent flowing slowly through a tube. *Proc. R. Soc. Lond.* A **219** (1137), 186–203.

WILLIAMS, M.S., LONGMUIR, K.J. & PAUL, Y. 2008 A practical guide to the staggered herringbone mixer. *Lab Chip* **8** (7), 1121–1129.

YARIV, E. & DORFMAN, K.D. 2007 Electrophoretic transport through channels of periodically varying cross section. *Phys. Fluids* **19** (3), 037101.

YOON, S. & KANG, P.K. 2021 Roughness, inertia, and diffusion effects on anomalous transport in rough channel flows. *Phys. Rev. Fluids* **6** (1), 014502.

ZHENG, C. & WANG, P.P. 1999 MT3DMS : a modular three-dimensional multispecies transport model for simulation of advection, dispersion, and chemical reactions of contaminants in groundwater systems; documentation and user's guide, pp. 1–3. Accepted: 2016-03-17T12:45:13Z Publisher: Environmental Laboratory (U.S.).

ZITSERMAN, V.Y., BEREZHKOVSKII, A.M., ANTIPOV, A.E. & MAKHNOVSKII, Y.A. 2014 Biased diffusion in tubes of alternating diameter: analytical treatment in the case of strong bias. *J. Chem. Phys.* **141** (21), 214103.